Stability-Constrained Settings of Directional Overcurrent Relays With Shifted User-Defined Characteristics for Distribution Networks With DERs

Ahmed N. Sheta , Bishoy E. Sedhom , *Member, IEEE*, Anamitra Pal , *Senior Member, IEEE*, Mohamed Shawky El Moursi , *Fellow, IEEE*, and Abdelfattah A. Eladl

Abstract—**Microgrids (MGs) with distributed energy resources (DERs) offer multiple advantages in terms of energy efficiency, reliability, and sustainability. However, due to the changes DERs bring to the fault currents, ensuring protection for DER-rich distribution grids is more challenging than conventional grids. This paper investigates the implementation of directional overcurrent relays (DOCRs) in MGs, considering the transient stability of the DERs. Given the low inertia of the DERs, the high operating times of DOCRs can potentially impede DERs' stability, even at post-fault. As such, this paper proposes a novel approach using shifted user-defined characteristics of DOCRs that employs two inverse curves to maintain both relay-relay coordination as well as DERs' stability. Then, the critical clearing times of DERs are combined with the coordination constraints to determine DOCR's optimal settings using genetic algorithm. The proposed methodology is evaluated using the modified IEEE 33-bus test system equipped with four synchronous-based DERs. DigSILENT and MATLAB are used to simulate the system, solve the optimization problem, and analyze transient stability. The results indicate the superior performance by the proposed characteristics in comparison with single characteristic to meet both relay coordination and DERs' stability requirements.**

Index Terms—**Critical clearing time, directional overcurrent relay, microgrid protection, relay coordination, and transient stability.**

I. INTRODUCTION

MICROGRID (MG) is a network of distributed energy resources (DERs) that can power appliances, while operating in standalone or grid-connected modes [1]. Although the contributions of MGs in terms of sustainability of supply, energy efficiency, and system reliability [2], they have been found to negatively affect existing protection systems due to the changes they bring to the short circuit levels. The changes depend on capacity, location, and operating mode and type of the DERs (inverter-based or synchronous-based) [3].

Particularly, directional overcurrent relays (DOCRs) have been very effective and reliable in protecting MGs because they can assess the magnitude and direction of fault currents before initiating trip commands. This feature is highly advantageous in MGs with intricate configurations featuring multiple current paths and sources [4]. However, achieving coordination among DOCRs in DER-rich distribution grids proves challenging due to the rise in fault currents associated with the involvement of DERs, especially synchronous-based ones. As the fault current rises, the operating time of DOCRs with inverse characteristics decreases, obstructing the effective coordination between primary and backup relays [5], [6]. In this context, different deterministic and heuristic optimization algorithms have been implemented to identify the optimal settings of DOCRs under various constraints in MGs [7], [8], [9], [10], [11], [12]. Despite the contributions of these studies to DOCR coordination, they have ignored the transient stability of DERs by assuming all DERs remain stable after the fault clearance. This assumption is problematic in MGs due to the susceptibility of DERs to instability after clearing the fault. In contrast to large synchronous machines in transmission systems, which benefit from ample inertia allowing relays to operate without impeding the system's stability, DERs in MGs have limited capacity, inertia and inherent damping. Therefore, disregarding transient stability considerations of DERs in DER-rich distribution grids may precipitate wide instability problems [13], [14], [15].

Some studies have examined the stability of DERs with coordination issues in DER-rich distribution grids [15], [16], [17], [18], [19], [20], [21]. In [15], equal area criteria was employed to define the critical clearing time (CCT) of DERs at different locations to identify optimal settings of DOCRs; however, relay-relay coordination was ignored in this study. In [16], a CCT analysis was conducted in a distribution network with synchronous-based DERs. However, DOCRs could not

respond quickly enough to preserve the stability of the generators during near-end faults. The authors in [17] used fuzzy logic to optimize the settings of DOCRs considering DERs' stability. They used the potential energy boundary surface and bisection methods to obtain the critical clearing time (CCT) of DERs. However, the approach was found to be time-consuming and less accurate. In [18], the authors employed a double-standard inverse relay characteristic for DOCRs. Despite the potential benefits of the double-inverse characteristics, this approach exhibited slow operation during high fault conditions, which impeded the system's stability. The standard-inverse characteristic of DOCRs was adjusted with suitable slopes in [19], to minimize relay operating times to preserve system stability. However, the authors neglected the consideration of the circuit breaker opening times. Furthermore, their method exhibited limitations in its ability to effectively handle far-end faults. References [20] and [21] presented a solution to the work in [18] by combining both definite-time and inverse-time characteristics. Although this hybrid approach provided a swifter response at high currents, definite time characteristics may demonstrate insensitivity to fault severity and insufficient discrimination between fault currents and high normal currents, such as inrush currents.

This paper proposes a novel approach for determining the optimal settings of DOCRs using genetic algorithm (GA) while considering both relay-relay coordination and the stability of synchronous-based DERs. The proposed method leverages the capabilities of digital relays, allowing for a wider range of choices and possibilities in achieving optimal DOCR settings. The study initially performs coordination of DOCRs without incorporating CCTs. Then, the need for considering stability of DERs within the optimization frame-work is highlighted. Next, the proposed method is developed by adjusting the coefficients of the inverse characteristic and employing upward and downward shifts, to provide fast operation of DOCRs while also maintaining stability of DERs. Lastly, a modified IEEE 33-bus system is used to evaluate the proposed method under various scenarios, including load reduction and transformer energization periods, to validate its effectiveness. The main contributions of this paper can be summarized as follows:

- Proposing a double-inverse DOCR setting to ensure relay coordination and transient stability of DERs at post-fault.
- Expanding digital DOCR capabilities with broader non-standard characteristics to suit diverse applications.
- Providing optimal operating times with the main curve for backup relay operation and high-speed operation with the auxiliary curve for primary relay operation.
- Ensuring high sensitivity to fault severity and accurate discrimination between fault currents and high normal currents such as inrush currents.

The rest of the paper follows the following structure: Section II discusses the concepts and formulations of the conventional coordination problem. Section III presents a brief survey of synchronous machine stability, and the analytical formulations used to find the CCT of these small-scale machines during fault conditions. Section IV outlines the proposed methodology to set DOCRs constrained by the stability of DERs. Section V shows the simulation analysis and provides a discussion of the results. Finally, Section VI concludes the findings of this paper.

TABLE I
TRIPPING CURVES' STANDARD COEFFICIENTS OF OVERCURRENT RELAYS

Relay curve type	A	B
Normally inverse	0.14	0.02
Very inverse	13.5	1
Extremely inverse	80	2

II. COORDINATION PROBLEM IN MGs

The optimal coordination of relays is usually determined by solving an optimization problem with an objective function and some constraints. The objective function is generally described as minimizing the total operating times of relays (T_{op}) during faults as described in (1) [7]. In this optimization problem, the decision variables refer to the settings of the individual relays. These settings typically include the time dial setting (TDS), as well as the pickup current (I_p).

$$\text{Minimize} \Rightarrow T_{op} = \sum_{f=1}^{f_{\max}} \left(\sum_{i=1}^{N} \left(t_i^{\text{PM}} + \sum_{j=1}^{J} t_{ij}^{\text{BK}} \right) \right) \quad (1)$$

where f indicates fault location, i refers to primary relays (PM) whose total number is N, j points to backup relays (BK) whose total number is J, t_i^{PM} denotes primary relay operating time, and t_{ij}^{BK} denotes backup relay operating time. Typically, the operating time (t) of overcurrent relays is related to the inverse time-current characteristics, as shown in (2),

$$t = TDS_i \frac{A}{\left(\frac{I_{f,i}}{I_{p,i}}\right)^B - 1} \quad (2)$$

where $I_{f,i}$ refers to the fault current through the relay i, $I_{p,i}$ represents relay's pickup current setting, A and B are values denoting the relay characteristics coefficients, with standard values as specified in Table I [21].

For effective relay coordination, it is essential to ensure that the relay settings meet the coordinating time interval (CTI). The CTI is the minimum time difference between the operation of backup and primary relays for any fault, with a recommended range of 0.2 to 0.5 seconds [5]. This constraint can be mathematically represented as shown in (3).

$$t_{ij}^{\text{BK}} - t_i^{\text{PM}} \geq \text{CTI}, \, \forall \, i, j \quad (3)$$

The pickup current value (I_p) for a relay i is determined using (4), which ensures that its lower value is greater than the rated load current (I_{Rl}) at the relay location. Additionally, it must not exceed the minimum fault current ($I_{f_{min}}$) sensed by the relay in its backup mode.

$$1.1 \cdot I_{Rl,i} \leq I_{P,i} \leq x \cdot I_{f_{min},i}, \, \forall \, i \quad (4)$$

where x is defined in (5) to maintain the upper limit of (I_p) greater than its lower limit [5].

$$x = \begin{cases} 0.6 \rightarrow if \ 0.6 \cdot I_{f_{min},i} \geq 1.1 \cdot I_{Rl,i} \\ 0.8 \rightarrow otherwise \end{cases} \quad (5)$$

The selection of the TDS for the relay i should also adhere to the guidelines outlined in (6), with lower and upper limits,
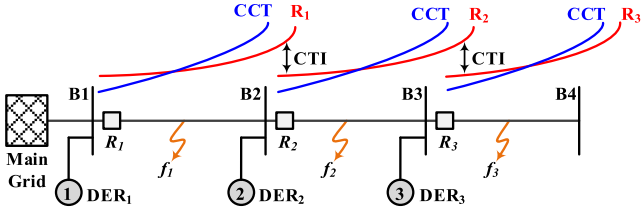
Fig. 1.   Relay time and CCT curves for a radial feeder with DERs.

Fig. 2.   P-δ curves for stability analysis of synchronous machines.

denoted as $\text{TDS}_{i,\,min}$ and $\text{TDS}_{i,\,max}$, respectively.

$$TDS_{i,min} \leq TDS_i \leq TDS_{i,max}, \ \forall \, i \qquad (6)$$

As seen, this formulation of the coordination problem does not account for the transient stability of DERs, which will be further discussed in the following sections.

III. TRANSIENT STABILITY ANALYSIS OF DERS

The integration of DERs in MGs significantly impacts the transient stability of the system. Unlike large synchronous machines, DERs, characterized by low inertia, limited capacity, and insufficient inherent damping, can face instability problems after faults are cleared, mainly due to the extended operation time of protective relays. To mitigate the likelihood of such undesirable events, it is crucial to consider the stability of DERs by incorporating new constraints into the formulation derived in Section II. This involves utilizing the CCT of DERs, which determines the maximum allowable duration for fault clearance to prevent system instability. Fig. 1 depicts a radial distribution system with three DERs to demonstrate the limitations posed by transient stability. It shows CCT and relay time curves at various locations. The CCT profile in this figure is influenced by the damping behavior of distribution line resistance, especially with greater damping at the end than at the beginning, causing a greater CCT at the end compared to the starting point [20]. In certain regions, the CCT is lower than the relay operating time, indicating the occurrence of unstable operation of upstream DERs in those areas following the clearance of faults. Conversely, in other regions, the CCT exceeds the operating time, indicating stable operation of DERs after fault clearance. For example, in the event of a fault occurrence (f_2), the sum of the operating times of the primary relay (R_2) and the opening time of the circuit breaker associated with that relay must be less than the CCT due to this fault. This ensures the stability of the upstream DERs (DER$_1$ and DER$_2$); otherwise, they will lose stability once the fault is cleared. Thus, to address this concern, the optimization problem must incorporate the CCT as a constraint on the operational time of the primary relays [21], as expressed in (7).

$$t_f^{PM} \leq CCT_f - t_{CB} \qquad (7)$$

where t_f^{PM} refers to the operating time of the primary relay for fault f, t_{CB} is circuit breaker's opening time, while CCT_f represents the CCT due to fault f. It is worth mentioning that, CCT_f is the minimum CCT value among all the upstream DERs affected by fault f, as defined in (8). This is because, following
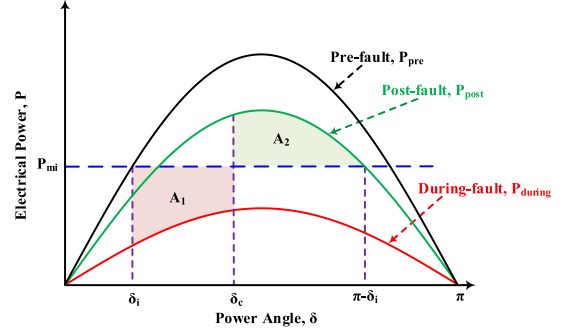
fault clearance, the DERs located downstream will be islanded and disconnected according to IEEE guidelines.

$$CCT_f = \min \left(CCT_{DER_1,f}, \ CCT_{DER_2,f}, \ \ldots, CCT_{DER_n,f} \right) \qquad (8)$$

where n represents the number of total upstream DERs to the fault f. For instance, in Fig. 1, when determining CCT_{f_2} only the CCT values of DER$_1$ and DER$_2$ are considered since they are located upstream of f_2, disregarding the stability of DER$_3$, which is downstream of f_2.

For synchronous machines, equal area criteria is used to find the CCT, as shown in Fig. 2. When a fault occurs at δ_i, the machine enters an acceleration phase characterized by a sudden decline in output power, defined by the during-fault curve and the acceleration area A_1. After the fault is cleared at δ_c, the output power experiences another abrupt change and follows the post-fault curve, resulting in energy dissipation during the deceleration phase denoted by the deceleration area A_2. Thus, the machine shows stable operation when $A_1 \leq A_2$, indicating that the fault is cleared at a power angle δ lower than the critical clearing angle δ_{CCT}. Analytically, the CCT can be calculated, for shown Fig. 2, using (9) and (10) [22].

$$\delta_{\text{CCT}} = \cos^{-1}$$
$$\times \left(\frac{P_{mi}\,(\pi - 2\delta_i) - P_{during} \cos \delta_i - P_{post} \cos \delta_i}{P_{post} - P_{during}} \right) \qquad (9)$$

$$\text{CCT} = \sqrt{\frac{2H}{(P_{mi} - P_{during})\pi f} \, (\delta_{CCT} - \delta_i)} \qquad (10)$$

where δ_{CCT} is the critical clearing angle, δ_i represents the initial load angle, H refers to the inertia constant, P_{mi} reflects the mechanical input power, and P_{during} and P_{post} define output power during and after fault, respectively. Indeed, the CCT formulas explained in (9) and (10) do not fully capture all fault scenarios (i.e., permanent and transient faults), system configurations (i.e., parallel lines), or regulating devices, which consequently result in distinct curves and equations when compared to the previously depicted ones [18]. This study conducts repeated time-domain simulations using DigSILENT software to obtain the CCTs at different fault points. For each relay, various faults are simulated within its protected zone. For each fault, the response time of

the relay (fault clearing time) is gradually increased in steps. At each step, the speed and power output of upstream DERs are analyzed to assess transient stability. The time after which any upstream DER to this simulated fault becomes unstable is designated as the CCT for this fault location. In this work, three phase permanent faults are adopted since they have the most severe impact on system stability [17].

IV. PROPOSED METHODOLOGY

As previously discussed, ensuring timely clearance of fault events before the CCT is crucial for preserving the stability of DERs. This operation is further constrained by the CTI among relays, allowing selective operation. For the system shown in Fig. 1, the coordination problem incorporates the following constraints to satisfy stability and selectivity requirements:

- CCT *constraints:*

$$t_{R_3, f_3} \leq CCT_{R_3, f_3} - t_{CB} \tag{11}$$

$$t_{R_2, f_2} \leq CCT_{R_2, f_2} - t_{CB} \tag{12}$$

$$t_{R_1, f_1} \leq CCT_{R_1, f_1} - t_{CB} \tag{13}$$

$$CCT_{R_3, f_3} = \min (CCT_{DER_1, f_3},$$
$$CCT_{DER_2, f_3}, CCT_{DER_3, f_3}) \tag{14}$$

$$CCT_{R_2, f_2} = \min (CCT_{DER_1, f_2}, CCT_{DER_2, f_2}) \tag{15}$$

$$CCT_{R_1, f_1} = (CCT_{DER_1, f_1}) \tag{16}$$

- CTI *constraints:*

$$t_{R_2, f_3} - t_{R_3, f_3} \geq CTI \tag{17}$$

$$t_{R_1, f_3} - t_{R_2, f_3} \geq CTI \tag{18}$$

$$t_{R_1, f_2} - t_{R_2, f_2} \geq CTI \tag{19}$$

Indeed, adopting a single characteristic, i.e., normal inverse, poses challenges in satisfying both CCT and CTI requirements. If the relay characteristic is chosen based on the CCT, the stability of DER will be maintained; however, this may impede coordination between primary and backup relays. Conversely, if the characteristics are selected to fulfill CTI considerations, it is possible that the DERs will become unstable. Consequently, a novel approach called the shifted user-defined-DOCR (SUD-DOCR) is proposed, employing two curves to address the CTI and DERs' stability simultaneously. The SUD-DOCR consists of the main and auxiliary curves, as depicted in Fig. 3.

As seen, in Fig. 3, the main curve is set using conventional settings (1) to (6), while the auxiliary curve is designed to rapidly trip high fault currents while ensuring the stability of DERs. The following subsections highlight the concepts of the SUD characteristics of DOCR.

A. User-Defined DOCR Characteristics

The coordination problem is traditionally addressed by assuming fixed values for the coefficients A and B, as outlined in Table I. However, the advancement of digital relays allows for the adjustment and customization of these coefficients by end-users. Consequently, in the proposed approach, both A and
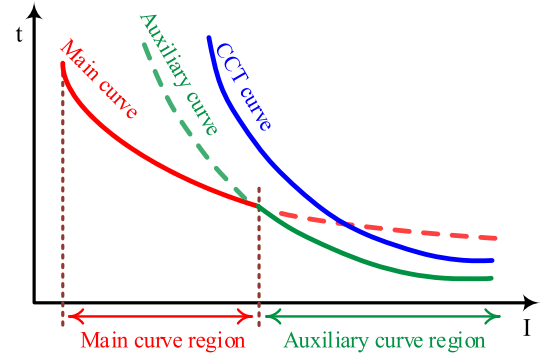

Fig. 3.   Characteristics of proposed main-auxiliary curve method.
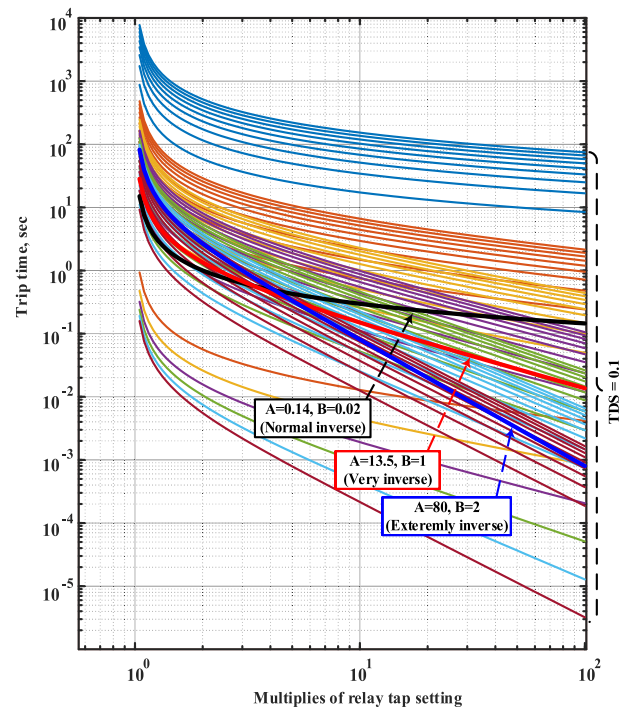

Fig. 4.   Variations in overcurrent relay characteristics with A and B adjustments.

B are treated as variables, offering enhanced flexibility within digital DOCRs. This enables the operation of DOCRs with a wide range of characteristics, surpassing the conventional ones [23]. It is clear from Fig. 4 that altering the values of A and B at a given TDS results in the emergence of different inverse characteristics, indicating the possibility of defining new curves beyond the conventional set of normal inverse, very inverse, and extremely inverse characteristics.

The optimal values of A and B for a given relay i can be determined by setting their upper and lower limits according to (20) and (21), respectively. In this study, the range of A_i is defined as [0.14, 80], representing the lower limit $A_{i,min}$ and upper limit $A_{i,max}$. Similarly, the range of B_i is considered as [0.02, 2], representing the lower limit $B_{i,min}$ and upper limit
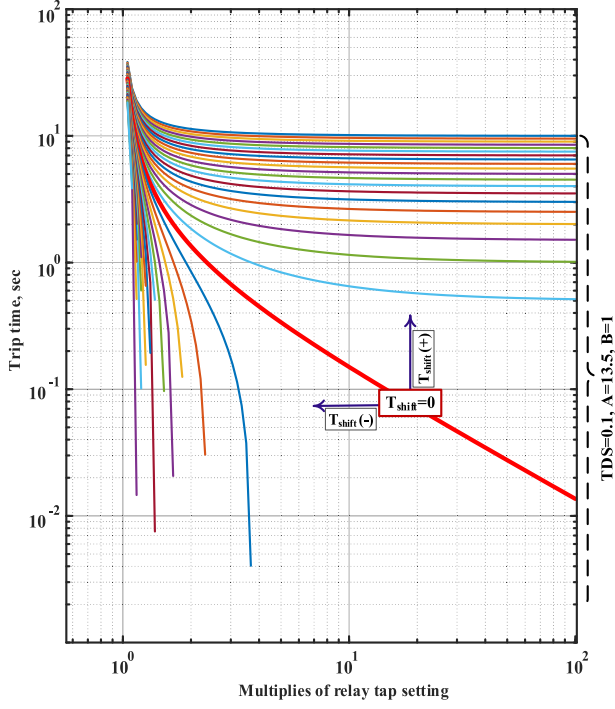
Fig. 5. Shifted overcurrent relay characteristics at constant TDS, A, and B.

Fig. 6. Flowchart of proposed method.

$B_{i,max}$ [23].

$$A_{i,min} \leq A_i \leq A_{i,max}, \ \forall \, i \tag{20}$$

$$B_{i,min} \leq B_i \leq B_{i,max}, \ \forall \, i \tag{21}$$

B. Shifted DOCR Characteristics

The emergence of digital relays has also empowered users to override the standard parameters of overcurrent relays. Alongside the flexible selection of A and B, it grants the capability to fine tune the relay's characteristics in a downward or upward manner by controlling a shifting value, denoted as T_{shift}. This adjustment serves the purpose of minimizing the relay's operating time, facilitating optimal coordination among multiple relays [24]. This upward and downward shifting can be defined as shown in (22),

$$t_{aux} = TDS_i \frac{A_i}{\left(\frac{I_{f,i}}{I_{p,i}}\right)^{B_i} - 1} + T_{shift} \tag{22}$$

where T_{shift} represents a shifting factor that plays a crucial role in enabling viable solutions for resolving coordination issues. As mentioned in [24], the typical range for the T_{shift} factor is between -10 and 10, ensuring the generation of feasible solutions. Fig. 5 illustrates the influence of varying T_{shift} while keeping the values of TDS, A, and B constant. It demonstrates that this shifting factor leads to the creation of additional characteristics that significantly contribute to accomplishing the objectives of this study.

This paper combines variations in coefficients A and B with characteristics shifting (T_{shift}) to offer a comprehensive set of choices and p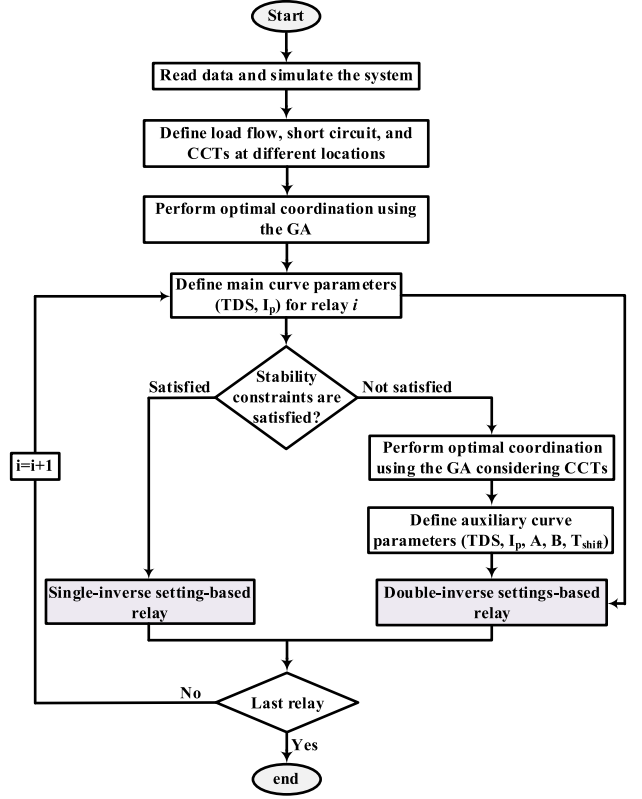ossibilities for achieving optimal performance and customization in DOCR settings. For the auxiliary curve, the modified objective function and constraints are defined as follows:

$$\text{Minimize} \Rightarrow T_{op,aux} = \sum_{f=1}^{f_{max}} \left(\sum_{i=1}^{N} \left(t_{aux,i}^{PM} + \sum_{j=1}^{J} t_{aux,ij}^{BK} \right) \right) \tag{23}$$

Subjected to,

$$t_{aux} = TDS_{aux,i} \frac{A_{aux,i}}{\left(\frac{I_{f,i}}{I_{Paux,i}}\right)^{B_{aux,i}} - 1} + T_{shift,i} \tag{24}$$

$$t_{aux,ij}^{BK} - t_{aux,i}^{PM} \geq CTI, \qquad \forall \, i,j \tag{25}$$

$$TDS_{i,min} \leq TDS_{aux,i} \leq TDS_{i,max}, \qquad \forall \, i \tag{26}$$

$$A_{i,min} \leq A_{aux,i} \leq A_{i,max}, \qquad \forall \, i \tag{27}$$

$$B_{i,min} \leq B_{aux,i} \leq B_{i,max}, \qquad \forall \, i \tag{28}$$

$$1.1 \cdot I_{Rl,i} \leq I_{Paux,i} \leq x \cdot I_{fmin,i}, \qquad \forall \, i \tag{29}$$

$$T_{shift,i,min} \leq T_{shift,i} \leq T_{shift,i,max}, \qquad \forall \, i \tag{30}$$

$$t_{aux,f}^{PM} \leq CCT_f - t_{CB} \tag{31}$$

In this study, circuit breaker time, t_{CB}, is considered to be 0.025 seconds [18]. Fig. 6 depicts the flowchart of the proposed protection coordination scheme.
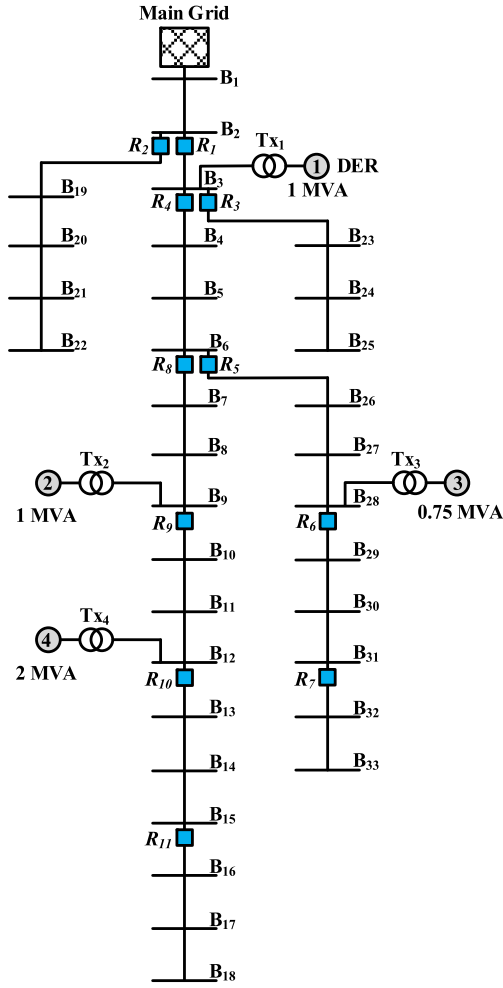
Fig. 7. The modified IEEE 33-bus test system.

Relay No.	I_P (A)	TDS	Relay No.	I_P (A)	TDS
1	152.40	0.3	7	17.64	0.05
2	28.80	0.05	8	68.40	0.28
3	54.48	0.05	9	47.88	0.23
4	120.60	0.29	10	67.08	0.12
5	32.04	0.27	11	28.32	0.05
6	44.76	0.15			

for $\text{TDS}_{i,\,min}$ and $\text{TDS}_{i,\,max}$ is set to 0.35 [5]. It is worth noting that changes in system topology, DER placement, or DER type (e.g., synchronous-based or inverter-based), will impact system currents, CCTs, and, consequently relay settings. While this study focuses on the examined scenario for brevity, the proposed algorithm can be applied to other scenarios having new currents and CCTs.

This study investigates the effectiveness of the proposed method by conducting simulations considering the following:

- *Conventional coordination of DOCRs:* The coordination of DOCRs is done using normal inverse characteristics without including CCTs. The resulting settings are then assessed by comparing them with the CCT curves.
- *DOCRs settings with/without considering DERs:* This section investigates the impact of DERs connection on relay settings.
- *Proposed SUD-DOCR method:* Stability constraints are included in the coordination problem, where DOCRs are set according to the proposed method.
- *Variation of system loading:* The proposed method's performance is examined under variable power produced by DERs during off-peak periods. This involves a 10% reduction in all the loads.
- *Transformer inrush current:* The proposed method's immunity against inrush currents is examined.
- *Recloser, fuse, and relay coordination:* The coordination between auto-reclosers, fuses, and relays is investigated.

A. Conventional Coordination of DOCRs

In this case, the optimal relay coordination problem does not consider the CCT constraints. Instead, only the CTI between primary and backup relays is used as a constraint. The optimal settings for this scenario using GA are presented in Table II.

The settings given in Table II show that each of the relays, namely R_2, R_3, R_7, and R_{11}, exhibits a rapid response with a TDS value of 0.05, exempting them from the need for CCT constraints without impeding their upstream DERs' stability. Notably, the location of R_1 with no upstream DERs allows its operating time to remain unconstrained by the CCT of any DER. To evaluate the settings of the remaining DOCRs, Fig. 8 illustrates their operating times based on the settings provided in Table II, alongside the CCTs at various locations within their primary zones. For instance, the CCT at R_4 for a near-end fault (NEF), at fault current equals 1.2 kA, is approximately 200 ms, and around 270 ms for a far-end fault (FEF), at fault current equals 1.02 kA, as shown in Fig. 8(a). Similarly, the CCT at R_5 for NEF is about 190 ms, and around 260 ms for FEF, as shown

V. RESULTS AND DISCUSSION

The suggested protection scheme is evaluated on a modified IEEE 33-bus system, equipped with four synchronous-based DERs and 11-DOCRs, as depicted in Fig. 7. The parameters of DERs are given in the Appendix with details in [20], while the mathematical models for the system elements are described in the DIgSILENT user manual [25]. Notably, any fault is isolated within this system by opening the corresponding upstream relays and anti-islanding protection of downstream DERs. DigSILENT and MATLAB software are employed to simulate the system, while the optimization problem is solved using GA. This study includes simulating different faults at various locations to determine the CCT values within relays' zones. For each fault, the operating time of the relevant relay is increased in steps. At each interval, the stability of all upstream DERs is checked. The goal is to pinpoint the operating time at which any of the upstream DERs becomes unstable. This time indicates the CCT for this particular location. These CCT values denote the maximum clearing time for all upstream DERs to maintain stability. For this study, a CTI value of 0.2 seconds has been selected, while for the ith relay, a value of 0.05 is selected
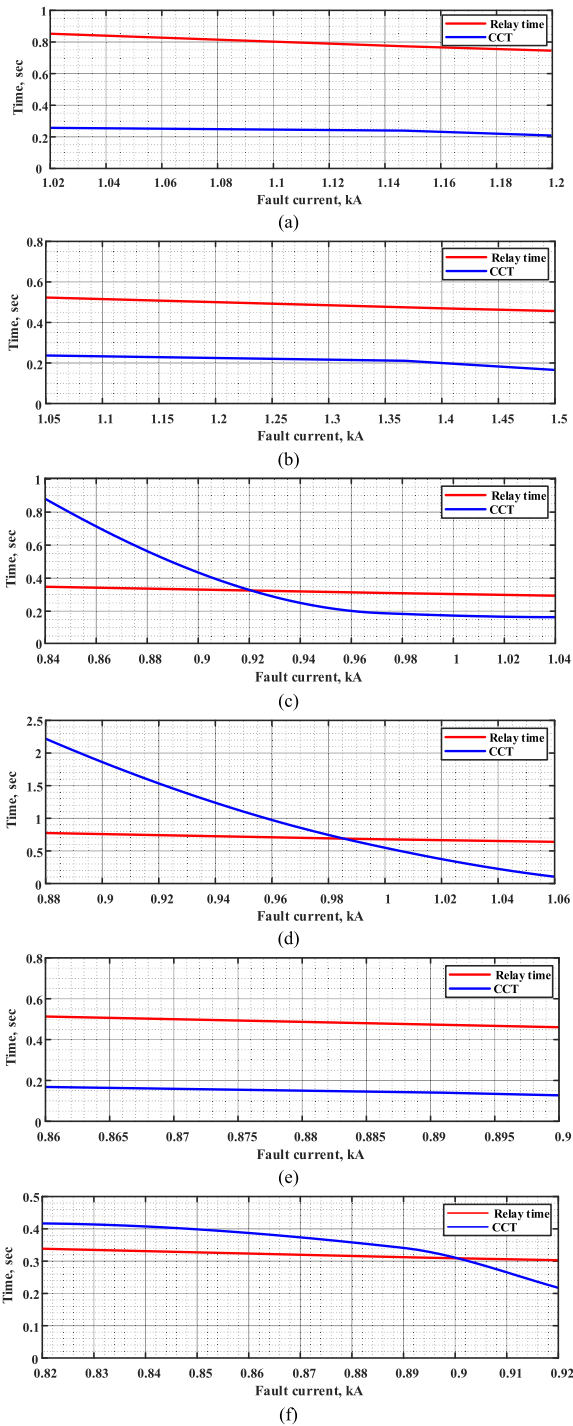
Fig. 8. Relays operating times and corresponding CCT curves (a) R_4; (b) R_5; (c) R_6; (d) R_8; (e) R_9; and (f) R_{10}.

TABLE III
OPTIMAL SETTINGS OF DOCRS (WITHOUT DERS)

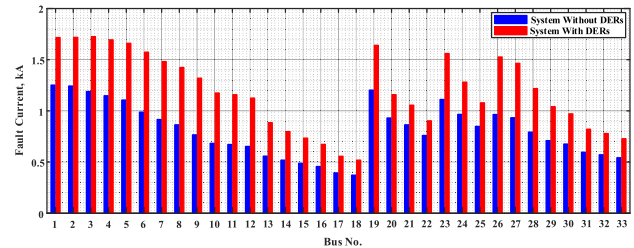| Relay No.	I_P (A)	TDS	Relay No.	I_P (A)	TDS
1	395.76	0.11	7	19.20	0.05
2	28.81	0.05	8	202.56	0.11
3	55.44	0.05	9	129.72	0.1
4	308.04	0.1	10	76.92	0.07
5	83.28	0.14	11	32.64	0.05
6	48.48	0.1			

Fig. 9. Fault current at different buses with/without considering DERs.

upstream DERs for faults within this region. Conversely, on the left of the intersection, the operating time falls below the CCT, indicating stable operation of upstream DERs when faults occur within this area. These findings emphasize the need for careful evaluation and adjustment of relay settings to ensure the stable operation of DERs and MGs.

B. DOCRs Settings With/Without Considering DERs

This section investigates the impact of DER connections on relay settings. Notably, when the DERs are absent, stability-constrained settings are irrelevant, so only main curve settings are defined for further analysis. This is because the main grid is assumed to have considerable inertia, resulting in higher CCT compared to DERs [18], [20], [21]. Table III shows DOCR settings without DERs, while Table II outlined the settings considering DERs.

Compared to Tables II, III shows significant changes in DOCR pickup values. This is because the main grid becomes the primary power provider, making relays witness higher normal currents when feeding downstream loads. Also, the settings outlined in Table III may prove unsuitable when DERs are considered, as their connection increases fault currents as shown in Fig. 9, affecting relay coordination. For instance, the settings in Table III are used to ascertain the operating times of both primary and backup relays for faults at various buses subsequent to DER connection. The timing relationships among primary, first-backup, and second-backup relays is depicted in Fig. 10. It shows compromised coordination among primary and backup relays, specifically (R_{11} and R_{10}), (R_6 and R_5), and (R_7 and R_6) for faults at B_{18}, B_{31}, and B_{33}, respectively.

C. Proposed SUD-DOCR Method

In this scenario, the coordination problem considers stability constraints to ascertain the optimal parameters of auxiliary curves for relays facing challenges with CCTs. The adjusted settings of these relays are outlined in Table IV, while the

in Fig. 8(b). It is clear from Fig. 8 that the operating times of R_4, R_5, and R_9, exceed their respective CCTs, suggesting potential instability for upstream DERs under conventional settings. Also, the operating times of relays R_6, R_8, and R_{10} intersect with CCT curves, indicating a critical zone where the upstream DERs may experience instability. On intersection's right side, the operating time exceeds the CCT, implying instability for the
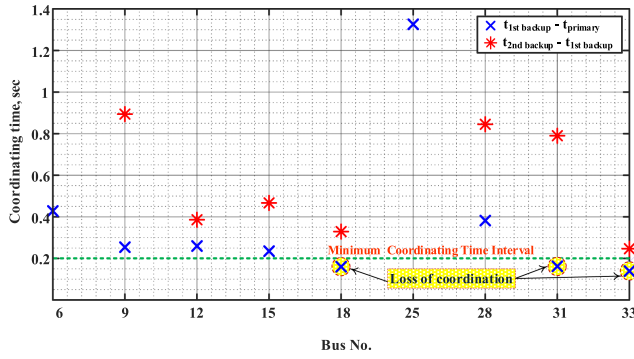
Fig. 10.   Operating time difference between primary and backup DOCRs.

TABLE IV
AUXILIARY CURVES OPTIMAL SETTINGS BASED ON THE PROPOSED METHOD

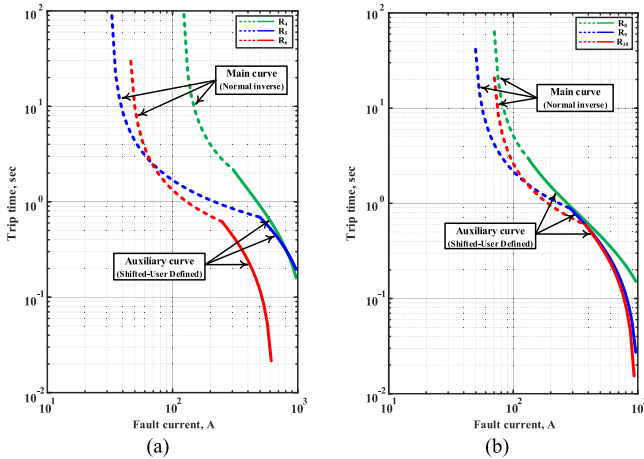| Relay No.	Ip (A)	TDS	A	B	T_{shift}
4	120.6000	0.3027	0.2534	0.0226	-1.4037
5	33.0888	0.1174	1.3652	0.0239	-1.6745
6	46.2601	0.3254	0.2519	0.0246	-0.8752
8	68.4015	0.2278	0.2401	0.0221	-0.7431
9	48.1152	0.2618	0.3771	0.0261	-1.1707
10	67.0844	0.3288	0.1937	0.0215	-1.0784

Fig. 11.   Proposed characteristics for (a) R_4, R_5, and R_6; (b) R_8, R_9, and R_{10}.

TABLE V
OPERATING TIMES OF RELAYS ACCORDING TO SETTINGS OF TABLE IV

Relay No.	Relay operating time (sec)		Relay No.	Relay operating time (sec)	
	NEF	FEF		NEF	FEF
4	0.035	0.148	8	0.133	0.199
5	0.005	0.186	9	0.072	0.092
6	0.155	0.234	10	0.021	0.073

proposed curves are in Fig. 11. Adopting the new settings yields a substantial reduction in the operational time of these relays at both NEF and FEF, as indicated in Table V.

A comparison of the operating times in Table V with the CCTs in Fig. 8 for corresponding faults highlights the effectiveness of the proposed methodology in ensuring the stable operation of DERs after faults are cleared. Implementing the SUD-DOCR
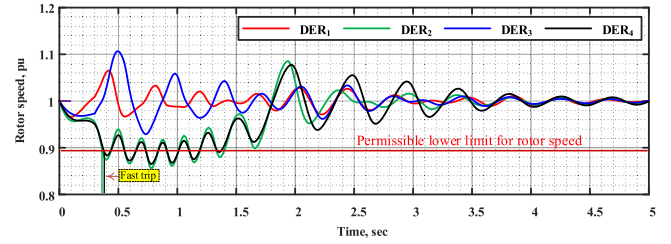
Fig. 12.   Rotor speeds for NEF to R_6 cleared using conventional setting.
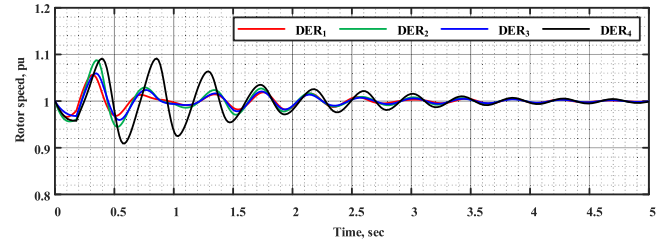
Fig. 13.   Rotor speeds for NEF to R_6 cleared using proposed method.

method significantly reduces relay operating times, thereby improving effectiveness. To illustrate this, a fault at the NEF to R_6 is examined. The setting of this relay considers the minimum CCT value of all DERs that are located to its upstream (namely, DER$_1$ to DER$_4$). Using the SUD-DOCR method, R_6 clears the fault within 180 ms, considering a breaker opening time of 25 ms. This swift response is facilitated by the rapid behavior exhibited by the auxiliary curve of the relay. In contrast, the conventional setting of R_6 mentioned in Table II, would result in a relay trip time of approximately 300 ms for this fault, as shown in Fig. 8(c), which exceeds the CCT of 200 ms. Figs. 12 and 13 display the rotor speeds of upstream DERs to this fault for different operating times of R_6. When the conventional-single curve setting is employed, the extended fault clearing time (300 ms) leads to instability of DER$_2$ and DER$_4$, as depicted in Fig. 12. Although the rotor speeds of DER$_2$ and DER$_4$ in Fig. 12 return to their pre-fault conditions, the recovery time is long (around 2 seconds). During this timeframe, the permissible lower limit for rotor speed (0.8963 pu) is violated [26], necessitating the fast trip of these DERs. Conversely, adopting the proposed SUD-DOCR method keeps all DERs remain connected to the grid and exhibit stable performance after fault clearance, as shown in Fig. 13. This confirms the benefits of the SUD-DOCR approach in maintaining DER stability during and after fault events.

D. Variation of System Loading

In this case, the performance of the proposed method is investigated under variable power produced by DERs during instances of load deviation from peak levels (off-peak periods). Consequently, these variations induce noteworthy changes in system currents and transient stability. In terms of transient stability, the CCT values are expected to be higher compared to those depicted in Fig. 8. This is attributed to the load reduction,
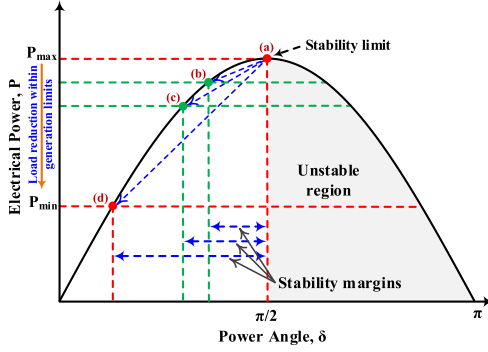
Fig. 14. P-δ curve for stability analysis during load variation.

TABLE VI
OPTIMAL SETTINGS OF DOCR MAIN CURVES WITH 10% LOAD REDUCTION

Relay No.	I_P (A)	TDS	Relay No.	I_P (A)	TDS
1	121.44	0.28	7	15.84	0.05
2	25.92	0.05	8	51.48	0.22
3	48.96	0.05	9	37.92	0.19
4	96.48	0.25	10	59.88	0.11
5	26.16	0.23	11	25.32	0.05
6	40.08	0.12			

TABLE VII
OPTIMAL SETTINGS OF DOCR AUXILIARY CURVES WITH 10% LOAD
REDUCTION

Relay No.	I_P (A)	TDS	A	B	T_{shift}
4	98.2608	0.3344	0.2730	0.0251	−1.2707
5	26.2806	0.1188	1.0963	0.0200	−1.4673
6	40.3302	0.3434	0.2592	0.0287	−0.7367
8	51.6049	0.3049	0.2484	0.0287	−0.6263
9	38.8285	0.3072	0.4334	0.0361	−0.9752
10	60.8185	0.3436	0.2608	0.0310	−0.9722

which leads to synchronous machines being moved away from critical points (stability limit) as shown in Fig. 14 [27]. This figure illustrates that the stability margin increases as the load on the generator is reduced, denoted by the transition from scenarios (a) to (b), (c), or (d), which corresponds to the minimum output of the respective generator. To simulate this scenario, a 10% reduction in all loads of the test system is applied. Fig. 15 compares CCT values for the test system with the 10% load reduction, contrasted against the values of normal loading conditions in Fig. 8. As previously discussed, the CCT values are observed to increase with load reduction.

The new relay settings that adapt the extended CCT values and current variations in this scenario are outlined in Tables VI and VII. Additionally, Fig. 16 visually represents the adjustments made to the DOCRs settings, effectively accommodating the specified changes in the system. The comparison of relay settings in Tables VI and VII with their counterparts in Tables II and IV demonstrates the reduction in pickup currents by different percentages, depending on the location of the relays. Moreover, the proposed method also makes further adjustments to other distinct parameters, such as TDS, A, B, and T_{shift} of DOCRs, to accommodate the changes in load conditions. Subsequently, the analysis of DOCRs settings depicted in Fig. 16(a) and (b),
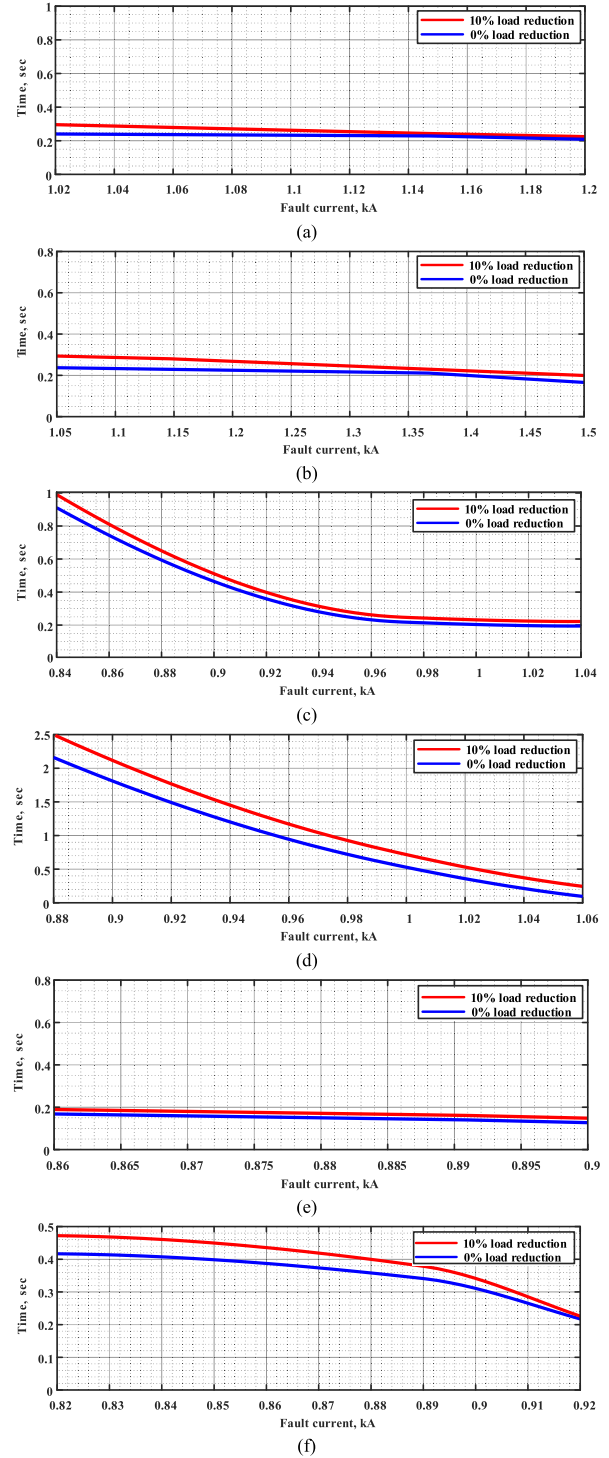

Fig. 15. CCT curves for 10% load reduction and normal loading for (a) R_4; (b) R_5; (c) R_6; (d) R_8; (e) R_9; and (f) R_{10}.

compared to their corresponding settings in Fig. 11(a) and (b), exhibits a notable disparity in the occupied operational range on the time-current curve during load reduction occurrences, as presented in Fig. 17.

Fig. 17 shows R_4 settings with/without load reduction. It illustrates that the auxiliary-fast curve covers a smaller region
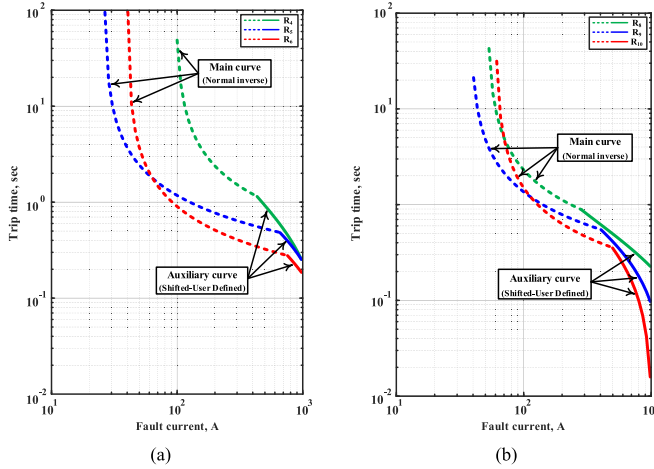
Fig. 16. Proposed settings at 10% load reduction for (a) R_4, R_5, and R_6; (b) R_8, R_9, and R_{10}.
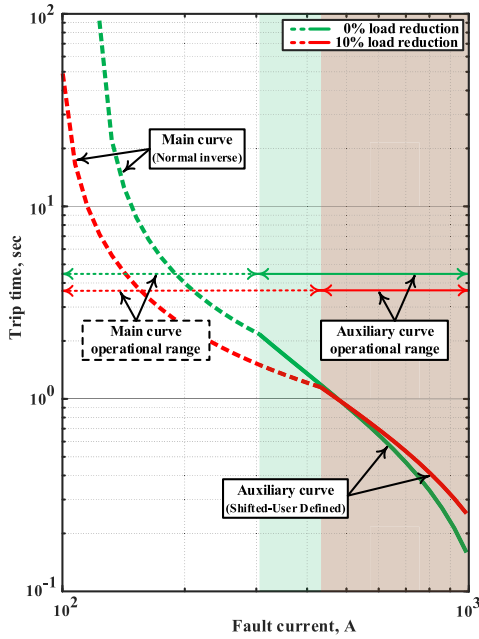

Fig. 17. Comparison of R_4 characteristics at 0% and 10% load reduction.

during the 10% load reduction compared to that of the 0% load reduction. Consequently, the main curve covers a greater operational area, leading to slower operating times for the DOCRs which is acceptable with higher CCTs. These findings reveals that as the system moves further away from peak periods, the CCTs tend to increase up to a certain limit, rendering the adoption of single curve setting (i.e., the main curve setting), a suitable approach to ensure both relay coordination and system stability after fault clearance.

E. Immunity Against Inrush Currents

This section evaluates the immunity of the proposed method during the energization period of transformers. In this period,

TABLE VIII
DOCR OPERATING TIMES FOR TRANSFORMER INRUSH CURRENTS

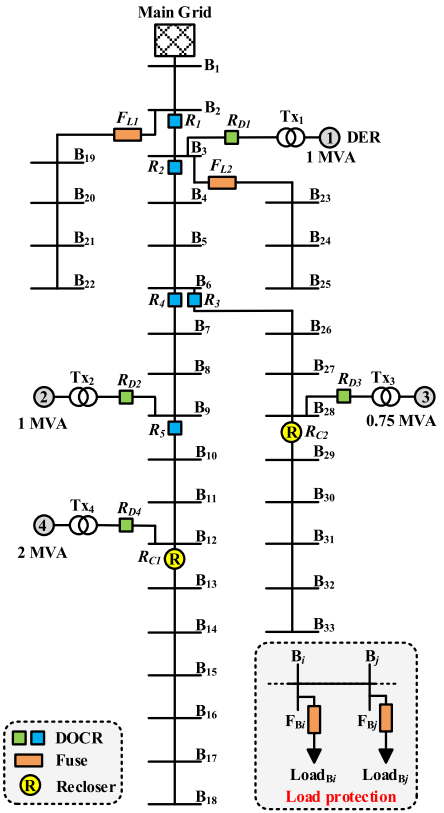| Transformer	Primary DOCR	Operating curve type	Relay operating time (sec)
Tx_1	R_1	Main curve	2.11
Tx_2	R_8	Auxiliary curve	0.753
Tx_3	R_5	Main curve	0.780
Tx_4	R_9	Auxiliary curve	0.463

Fig. 18. The test system considering DER protection, fuses, and reclosers.

transformers generally draw high currents, namely inrush currents that typically range from 8–12 times the transformer full load current and last for approximately 0.1 seconds [28]. The transient nature of these currents raises concerns about the potential false tripping of the relays. To this end, this study defines the operating times of primary DOCRs aligned with the inrush current magnitudes associated with the transformers shown in Fig. 7(Tx_1-Tx_4), as represented in Table VIII. Overall, the obtained results, in Table VIII, reveal that the operating times of DOCRs exceed the duration of the inrush currents (0.1 seconds), highlighting the proposed method's effectiveness during transformer energization periods.

F. Recloser, Fuse, and Relay Coordination

In this section, the proposed method is evaluated for a system equipped with reclosers, fuses, and relays, for load, feeder and DER protection. Fig. 18 depicts a modified IEEE 33-bus system equipped with 5 DOCRs ($R_1 - R_5$), 2 reclosers ($R_{C1} - R_{C2}$), and 2 line fuses ($F_{L1} - F_{L2}$) for feeder protection, 32 load fuses

TABLE IX
CHOSEN FUSES FROM S&C COMPANY STANDARD LIST

Fuse name	Specification
$F_{B6}, F_{B12}, F_{B15}, F_{B17}, F_{B18}, F_{B19}, F_{B23}, F_{B28}, F_{B33}$	6K
$F_{B5}, F_{B20}, F_{B21}, F_{B22}, F_{B29}, F_{B31}$	8K
F_{B4}, F_{B30}	10K
$F_{B2}, F_{B13}, F_{B26}, F_{B27}, F_{B32}$	15K
$F_{B8}, F_{B10}, F_{B14}, F_{B16}$	20K
$F_{B7}, F_{B9}, F_{B11}, F_{B24}, F_{B25}$	25K
F_{L1}	30K
F_{B3}	40K
F_{L2}	65K

TABLE X
SETTINGS OF DOCRs AND RECLOSERS OF THE SYSTEM IN FIG. 18

Relay No.	Main curve settings		Auxiliary curve settings				
	I_P (A)	TDS	I_P (A)	TDS	A	B	T_{shift}
R_1	152.4	0.229	---				
R_2	120.6	0.216	120.97	0.203	0.567	0.025	-1.745
R_3	32.04	0.205	33.29	0.174	0.818	0.023	-1.397
R_4	68.4	0.208	69.59	0.118	0.895	0.02	-1.716
R_5	47.88	0.168	49.39	0.093	1.619	0.021	-2.126
R_{C1}-Slow	67.08	0.081	67.08	0.05	0.14	0.02	0
R_{C1} - Fast	67.08	Instantaneous	---				
R_{C2} - Slow	44.76	0.097	44.76	0.05	0.14	0.02	0
R_{C2} - Fast	44.76	Instantaneous	---				
R_{D1}	54.73	0.05	---				
R_{D2}	54.73	0.05	---				
R_{D3}	41.04	0.05	---				
R_{D4}	109.45	0.05	---				

($F_{B2} - F_{B33}$) for load protection, and 4 DOCR ($R_{D1} - R_{D4}$) for DER protection. The coordination principles of these protective elements are briefly outlined below [29].

1) Fuse-Fuse Coordination: To coordinate fuses, the primary fuse must be faster than the backup fuse. The primary fuse's maximum clearing time (MCT) should not exceed 75% of the backup fuse's minimum melting time (MMT). This is to consider factors such as load current, ambient temperature, and fuse wear. Notably, the current rating of a fuse, which is the amount of current that the fuse can safely handle before it blows, can be determined by allowing a 20% overload [29]. This study selects fuses from the available list from S&C company for type-K fuse links [30], known for their fast response compared to other types such as type-T. Table IX outlines the specifications of the chosen fuses.

2) Relay-Recloser-Fuse Coordination: Reclosers uses dual time-current curves: a fast-tripping one for temporary faults and a delayed-tripping one for permanent faults. Typically, the fast curve operates first for high currents, protecting equipment and minimizing outages, while the slow curve enables downstream devices (e.g., fuses) to isolate faults, preventing unnecessary outages. Thus, the fuse's MMT should exceed the recloser's fast curve, while the fuse's MCT should be less than the recloser's slow curve. This study establishes the recloser's slow curve using the proposed SUD-DOCR scheme. However, for selecting an appropriate fast curve to meet the MMT requirements of fuses, the fast curve is set to respond instantaneously. It is important to highlight that effective relay-recloser coordination requires coordinating the recloser's slow curve with the DOCRs and

DER-CCTs, as outlined in Section IV. Moreover, since DOCRs $R_{D1} - R_{D4}$ are used for DER protection, they are designated with a TDS of 0.05 to ensure a fast response. Their pickup values are selected to exceed the DER's nominal current by 20%. Table X outlines the settings of DOCRs and reclosers of the system shown in Fig. 18.

VI. CONCLUSION

This paper proposes a novel stability-constrained protection coordination method for DOCRs in MGs with synchronous-based DERs. The method employs a dual-inverse characteristic, comprising a main curve and an auxiliary curve, to ensure efficient relay-relay coordination and DERs' transient stability. Evaluation on a modified IEEE 33-bus system demonstrated the superior performance of the proposed approach, reducing relay operating times by approximately 82% for near-end faults and 69% for far-end faults compared to single curve settings. The analysis also shows how off-peak load periods improve system stability, enabling the main curve, with its slower response, to serve as the primary setting instead of the faster auxiliary curve. Furthermore, the study evaluates the settings' immunity against high normal currents, such as inrush currents, revealing higher operating times of DOCRs during transient currents, surpassing the energization period by over 78%. The proposed scheme is also evaluated for relay-recloser-fuse coordination, fulfilling both the stability and coordination constraints. Building on the promising results of the proposed method, future research will investigate its robustness under different operating conditions and its adaptation to the rising number of inverter-based DERs with different characteristics. Moreover, it will investigate the coordination with anti-islanding protection and other relays, to maintain reliable and stable MG operation.

APPENDIX

The parameters of the main grid, DERs, and transformers are described below [20]:

Main Grid: MVA_{sc} = 20 MVA, Rated voltage = 12.66 kV.

Transformers: DER MVA rating, 12.66/3 kV, short circuit voltage (u_k) = 6%, X/R ratio = 8.5.

DERs: Rated voltage = 3 kV, inertia time constant (H) = DER's nominal MVA, r_{str}= 0.09 pu, x_l = 0.14 pu, $x_d = x_q$ = 1.55 pu, x'_d = 0.25 pu, x'_q = 0.6 pu, x''_d = 0.2 pu, x''_q = 0.6 pu, T'_d= 1 pu, T'_q= 1 pu, T''_d= 0.05 pu, T''_q= 0.05 pu.

REFERENCES

[1] P. Barra, D. Coury, and R. Fernandes, "A survey on adaptive protection of microgrids and distribution systems with distributed generators," *Renewable Sustain. Energy Rev.*, vol. 118, 2020, Art. no. 109524, doi: 10.1016/j.rser.2019.109524.

[2] S. Gopalan, V. Sreeram, and H. Iu, "A review of coordination strategies and protection schemes for microgrids," *Renewable Sustain. Energy Rev.*, vol. 32, pp. 222–228, 2014, doi: 0.1016/j.rser.2014.01.037.

[3] A. Sheta, G. Abdulsalam, B. Sedhom, and A. Eladl, "Comparative framework for AC-microgrid protection schemes: Challenges, solutions, real applications, and future trends," *Protection Control Modern Power Syst.*, vol. 8, pp. 1–40, 2023, doi: 10.1186/s41601-023-00296-9.

[4] N. Hussain, M. Nasir, J. Vasquez, and J. Guerrero, "Recent developments and challenges on AC microgrids fault detection and protection systems–A review," *Energies*, vol. 13, 2020, Art. no. 2149, doi: 10.3390/en13092149.

[5] H. Beder, B. Mohandes, M. S. E. Moursi, E. A. Badran, and M. M. E. Saadawi, "A new communication-free dual setting protection coordination of microgrid," *IEEE Trans. Power Del.*, vol. 36, no. 4, pp. 2446–2458, Aug. 2021, doi: 10.1109/TPWRD.2020.3041753.

[6] H. M. Sharaf, H. H. Zeineldin, and E. El-Saadany, "Protection coordination for microgrids with grid-connected and islanded capabilities using communication assisted dual setting directional overcurrent relays," *IEEE Trans. Smart Grid*, vol. 9, no. 1, pp. 143–151, Jan. 2018, doi: 10.1109/TSG.2016.2546961.

[7] E. Dehghanpour, H. Kazemi Karegar, R. Kheirollahi, and T. Soleymani, "Optimal coordination of directional overcurrent relays in microgrids by using cuckoo-linear optimization algorithm and fault current limiter," *IEEE Trans. Smart Grid*, vol. 9, no. 2, pp. 1365–1375, Mar. 2018, doi: 10.1109/TSG.2016.2587725.

[8] T. E. Sati and M. A. Azzouz, "Optimal protection coordination for inverter dominated islanded microgrids considering N-1 contingency," *IEEE Trans. Power Del.*, vol. 37, no. 3, pp. 2256–2267, Jun. 2022, doi: 10.1109/TPWRD.2021.3108760.

[9] S. Asl, M. Gandomkar, and J. Nikoukar, "Optimal protection coordination in the micro-grid including inverter-based distributed generations and energy storage system with considering grid-connected and islanded modes," *Electric Power Syst. Res.*, vol. 184, 2020, Art. no. 106317, doi: 10.1016/j.epsr.2020.106317.

[10] K. Sarwagya, P. Nayak, and S. Ranjan, "Optimal coordination of directional overcurrent relays in complex distribution networks using sine cosine algorithm," *Electric Power Syst. Res.*, vol. 187, 2020, Art. no. 106435, doi: 10.1016/j.epsr.2020.106435.

[11] A. Kachoee, H. Dezaki, and A. Ketabi, " Optimized adaptive protection coordination of microgrids by dual-setting directional overcurrent relays considering different topologies based on limited independent relays' setting groups," *Electric Power Syst. Res.*, vol. 214, 2023, Art. no. 108879, doi: 10.1016/j.epsr.2022.108879.

[12] J. Liang et al., "An improved inverse-time over-current protection method for a microgrid with optimized acceleration and coordination," *Energies*, vol. 13, 2020, Art. no. 5726, doi: 10.3390/en13215726.

[13] Y. Wang, J. Ravishankar, and T. Phung, "A study on critical clearing time (CCT) of micro-grids under fault conditions," *Renewable Energy*, vol. 95, pp. 381–395, 2016, doi: 10.1016/j.renene.2016.04.029.

[14] E. Mohamed, G. Magdy, G. Shabib, A. Elbaset, and Y. Mitani, "Digital coordination strategy of protection and frequency stability for an islanded microgrid," *IET Gener., Transmiss. Distrib.*, vol. 12, pp. 3637–3646, 2018, doi: 10.1049/iet-gtd.2018.0264.

[15] R. Razzaghi, M. Davarpanah, and M. Sanaye-Pasand, "A novel protective scheme to protect small-scale synchronous generators against transient instability," *IEEE Trans. Ind. Electron.*, vol. 60, no. 4, pp. 1659–1667, Apr. 2013, doi: 10.1109/TIE.2012.2186773.

[16] B. Keyvani, H. Nafisi, and H. Lesani, "Investigation on transient stability of an industrial network and relevant impact on over-current protection performance," in *Proc. IEEE 18th Elect. Power Distrib. Conf.*, 2013, pp. 1–6, doi: 10.1109/EPDC.2013.6565971.

[17] A. Momessoa, W. Bernardesb, and E. Asadaa, " Adaptive directional overcurrent protection considering stability constraint," *Electric Power Syst. Res.*, vol. 181, 2020, Art. no. 106190, doi: 10.1016/j.epsr.2019.106190.

[18] T. Soleymani Aghdam, H. Kazemi Karegar, and H. H. Zeineldin, "Optimal coordination of double-inverse overcurrent relays for stable operation of DGs," *IEEE Trans. Ind. Inform.*, vol. 15, no. 1, pp. 183–192, Jan. 2019, doi: 10.1109/TII.2018.2808264.

[19] A. Yazdaninejadi, D. Nazarpour, and S. Golshannavaz, "Sustainable electrification in critical infrastructure: Variable characteristics for overcurrent protection considering DG stability," *Sustain. Cities Soc.*, vol. 54, 2020, Art. no. 102022, doi: 10.1016/j.scs.2020.102022.

[20] T. S. Aghdam, H. Kazemi Karegar, and H. H. Zeineldin, "Transient stability constrained protection coordination for distribution systems with DG," *IEEE Trans. Smart Grid*, vol. 9, no. 6, pp. 5733–5741, Nov. 2018, doi: 10.1109/TSG.2017.2695378.

[21] A. Narimani and H. Dezaki, "Optimal stability-oriented protection coordination of smart grid's directional overcurrent relays based on optimized tripping characteristics in double-inverse model using high-set relay," *Int. J. Elect. Power Energy Syst.*, vol. 133, 2021, Art. no. 107249, doi: 10.1016/j.ijepes.2021.107249.

[22] Y. Sun, J. Ma, J. Kurths, and M. Zhan, "Equal-area criterion in power systems revisited," *Proc. Roy. Soc. A: Math., Phys. Eng. Sci.*, vol. 474, 2018, Art. no. 20170733, doi: 10.1098/rspa.2017.0733.

[23] J. Tripathi and S. Mallik, "An adaptive protection coordination strategy utilizing user-defined characteristics of DOCRs in a microgrid," *Electric Power Syst. Res.*, vol. 214, 2023, Art. no. 108900, doi: 10.1016/j.epsr.2022.108900.

[24] A. Fayoud, H. Sharaf, and D. Ibrahim, "Optimal coordination of DOCRs in interconnected networks using shifted user-defined two-level characteristics," *Int. J. Elect. Power Energy Syst.*, vol. 142, 2022, Art. no. 108298, doi: 10.1016/j.ijepes.2022.108298.

[25] "DIgSILENT PowerFactory version 15 user manual," Accessed: Feb. 25, 2024. [Online]. Available: https://http://www.digsilent.de

[26] S. Bharti, A. Sinha, A. Samantaray, and R. Bhattacharyya, "The Sommerfeld effect of second kind: Passage through parametric instability in a rotor with non-circular shaft and anisotropic flexible supports," *Nonlinear Dyn.*, vol. 100, pp. 3171–3197, 2020, doi: 10.1007/s11071-020-05681-9.

[27] M. Amroune and T. Bouktir, " Effects of different parameters on power system transient stability studies," *J. Adv. Sci. Appl. Eng.*, vol. 1, pp. 28–33, 2014.

[28] A. Draz, M. Elkholy, and A. El-Fergany, "Over-current relays coordination including practical constraints and DGs: Damage curves, inrush, and starting currents," *Sustainability*, vol. 14, 2022, Art. no. 2761, doi: 10.3390/su14052761.

[29] J. Gers and E. Holmes, "Fuses, reclosers and sectionalisers," in *Protection of Electricity Distribution Networks*, 3rd ed. London, U.K.: IET Digit. Library, 2011, ch. 6, pp. 125–146, doi: 10.1049/PBPO065E_ch6.

[30] "S&C electric company." Accessed: Feb.26, 2024. [Online]. Available: https://www.sandc.com

Ahmed N. Sheta was born in Egypt, in 1993. He received the B.Sc. and M.Sc. degrees in electrical engineering from Mansoura University, Mansoura, Egypt, in 2016 and 2020, respectively. He is currently working toward the Ph.D. degree with Electrical Engineering Department, Mansoura University. He is also a Researcher and an Assistant Lecturer with Electrical Engineering Department, Mansoura University. His research interests include power system protection and microgrids. In 2022, he was the recipient of the prestigious award for the best M.Sc. thesis at Mansoura University.

Bishoy E. Sedhom (Member, IEEE) received the B.Sc. (ranked first, with Hons.), M.Sc., and Ph.D. degrees in electrical engineering from the Faculty of Engineering—Mansoura University, Mansoura, Egypt. He is currently an Associate Professor with the Electrical Engineering Department, Mansoura University, Mansoura. His research interests include energy management, microgrid operation and control, power system protection, power quality, Internet of Things, optimization methods, islanding detection, system restoration, high voltage DC transmission grids, microgrid protection, smart manufacturing, and cybersecurity. He was the recipient of the best Ph.D. thesis award from Mansoura University in 2019, and University Encouragement Award from Mansoura University in 2023.

Anamitra Pal (Senior Member, IEEE) is currently an Associate Professor with the School of Electrical, Computer, and Energy Engineering, Arizona State University (ASU), Tempe, AZ, USA. His research interests include data analytics with a special emphasis on time-synchronized measurements, artificial intelligence-applications in power systems, renewable generation integration studies, and critical infrastructure resilience. Dr. Pal was the recipient of the 2018 Young CRITIS Award for his contributions to the field of critical infrastructure protection, 2019 Outstanding Young Professional Award from the IEEE Phoenix Section, National Science Foundation CAREER Award in 2022, and 2023 Centennial Professorship Award from ASU.

Mohamed Shawky El Moursi (Fellow, IEEE) received the B.Sc. and M.Sc. degrees in electrical engineering from Mansoura University, Mansoura, Egypt, in 1997 and 2002, respectively, and the Ph.D. degree in electrical engineering from the University of New Brunswick (UNB), Fredericton, NB, Canada, in 2005. In 2005, he joined Power Electronics Group, McGill University as a Postdoctoral Fellow. In 2006, he joined Vestas Wind Systems, where he worked on the Technology R&D with the Wind Power Plant Group, Arhus, Denmark, till October 2008. He was a Senior Study and Planning Engineer with TRANSCO, Abu Dhabi, UAE, till 2011. He is currently a Professor with Electrical Engineering Department and the Director of Advanced Power and Energy Center, Khalifa University, Abu Dhabi, and seconded to a distinguished Professor position with the Faculty of Engineering, Mansoura University. In 2012, he was a Visiting Professor with the Massachusetts Institute of Technology, Cambridge, MA, USA. His research interests include renewable energy integration, hybrid AC/DC power grid, FACTS technologies, VSC-HVDC systems, AC/DC Microgrid control, and AI applications in power systems. He is an IEEE Fellow (Class of 2024) for contributions to "Renewable Energy Integration and Hybrid Power Grids", and a Distinguished Lecturer of IEEE Power and Energy Society. He is also an Editor of IEEE TRANSACTIONS ON POWER DELIVERY, an Associate Editor for IEEE TRANSACTIONS ON POWER ELECTRONICS and IEEE TRANSACTIONS ON SMART GRID, Guest Editor of IEEE TRANSACTIONS ON ENERGY CONVERSION, Guest Editor-in-Chief for special section between TPWRD and TPWRS, Editor of IEEE POWER ENGINEERING LETTERS, Regional Editor of *IET Renewable Power Generation* and an Associate Editor for *IET Power Electronics Journals*. He was an Editor of IEEE TRANSACTIONS ON POWER SYSTEMS during 2017–2023.

Abdelfattah A. Eladl received the B.Sc. (ranked first, with Hons.), M.Sc., and Ph.D. degrees in electrical engineering from the Faculty of Engineering, Mansoura University, Mansoura, Egypt. His research interests include power system economics, protection, planning, smart grids, and energy hubs. He is currently an Associate Professor with the Electrical Engineering Department, Mansoura University. In 2016, he was the recipient of the Best Ph.D. Thesis Award from Mansoura University.